An annual cycle of Arctic surface cloud forcing at SHEBA

J. M. Intrieri,[1] C. W. Fairall,[1] M. D. Shupe,[2] P. O. G. Persson ,[3] E. L Andreas, [4] P. S. Guest ,[5] and R. E. Moritz [6]

Abstract. We present an analysis of surface fluxes and cloud forcing from data obtained during the Surface Heat Budget of the Arctic Ocean (SHEBA) Experiment, conducted in the Beaufort and Chuchki Seas and the Arctic Ocean from November 1997 to October 1998. The measurements used as part of this study include fluxes from optical radiometer sets, turbulent fluxes from an instrumented tower, cloud fraction from a depolarization lidar and ceilometer, and atmospheric temperature and humidity profiles from radiosondes. Clear sky radiative fluxes were modeled in order to estimate the cloud radiative forcing since direct observation of fluxes in cloud-free conditions created large statistical sampling errors. This was particularly true during summer when cloud fractions were typically very high. A year long data set of measurements, obtained on a multi-year ice floe at the SHEBA camp, was processed in 20 day blocks to produce the annual evolution of the surface cloud forcing components: upward, downward, and net longwave and shortwave radiative fluxes and turbulent (sensible and latent heat) fluxes. We found that clouds act to warm the Arctic surface for most of the annual cycle with a brief period of cooling in the middle of summer. Our best estimates for the annual average surface cloud forcings are -9 Wm^{-2} for shortwave, 38 Wm^{-2} for longwave, and -6 Wm^{-2} for turbulent fluxes. Total cloud forcing (the sum of all components) is about 30 Wm^{-2} for the fall, winter, and spring, dipping to a minimum of -4 Wm^{-2} in early July. We compare the results of this study with satellite, model, and drifting station data.

1. Introduction

According to many General Circulation Model simulations, the Arctic is predicted to show early warning indicators of changes in climate, and it is hypothesized that, with increasing levels of greenhouse gases, the polar regions will experience greater temperature changes than the tropical regions [*Washington and Meehl*, 1989]. This modeled warming is, in part, attributed to the *ice-albedo* (IA) feedback mechanism. However, not enough is known about the contemporary Arctic climate and its feedback mechanisms to predict or understand the implications of climate change. Various models account for polar processes in slightly different ways and, in some cases, yield vastly different climate simulations [e.g., *Randall et al.*, 1998; *Tao et al.*, 1996]. One point of consensus, however, is that the feedback with the largest potential impact involves clouds and that clouds significantly influence the way heat passes through the Arctic system.

Correctly incorporating Arctic cloud and surface properties, and their interdependence, into climate models is critical. The *cloud-radiation* (CR) feedback process is extremely complex in the Arctic region because of myriad functional dependencies that can be attributed to the underlying sea ice. For example, nonlinear relationships exist between Arctic clouds and the net surface flux which depend on surface conditions (a complicated fabric of ice, snow, melt pond, and open ocean waters). In turn, sea ice albedo and surface temperatures are strongly influenced by the presence of clouds and thus clouds indirectly affect boundary layer stability and latent and sensible heat fluxes [e.g., *Curry et al.*, 1996].

Thus far, model results have been our primary insight into the complexities and importance of polar cloud radiative effects [*Curry et al.*, 1993; *Curry et al.*, 1996] and have confirmed our need for better observations to correctly quantify the effects. The impact of Arctic clouds on the surface depends not only on cloud amount but also on cloud base height, the amount and phase of condensed water, particle size and shape, optical depth, and ice/water contents [e.g., *Curry and Ebert*, 1992]. *Curry et al.* [1993] conducted sensitivity studies in which they varied the properties of clouds and found that the mean thickness of Arctic sea ice was very sensitive to cloud characteristics. *Beesley* [2000] also examined the relationship between clouds and Arctic ice thickness using an energy budget and a single column model in which he incorporated thermodynamic coupling of the atmosphere and surface. He showed this coupling was essential and that local feedbacks can affect the dependence of ice thickness on cloud perturbations. Model results are insightful; however, understanding the role of clouds in the Arctic can be greatly improved by reliable observational estimates of cloud radiative forcing, especially as a function of cloud type and season [*Beesley*, 2000].

The lack of extensive observational information on IA and CR feedback processes motivated the Surface Heat Budget of the Arctic Ocean (SHEBA) field program [*Randall et al.*, 1998; *Perovich et al.*, 1999; *Curry et al.*, 2000]. SHEBA measurements included the annual cycle of all surface heat balance components (atmosphere, sea ice and ocean) for a multi-year ice floe. In this study, a comprehensive set of instruments was used to measure radiative and turbulent heat fluxes at the snow/ice - air interface [*Persson et al.*, 2001a,b] and ground-based remote sensing instruments, including a depolarization lidar, were used to measure cloud occurrence.

We used these observations to examine the impact of clouds on the surface energy balance over a complete annual cycle in the Arctic. Cloud

---

[1]NOAA/Environmental Technology Laboratory
Boulder, CO 80305
[2]Science and Technology Corporation
NOAA/Environmental Technology Laboratory
Boulder, CO 80305
[3]Cooperative Institute for the Environmental Sciences
NOAA/University of Colorado
Boulder, CO 80309
[4]U.S. Army Cold Regions Research and Engineering Laboratory
Hanover, NH
[5]Naval Postgraduate School
Monterey, CA
[6]Applied Physics Laboratory
University of Washington
Seattle, WA

radiative forcing (CRF), or the difference between the mean radiative flux and that which would be observed in the absence of clouds, has seen extensive application as an index of the importance of clouds in the global radiation balance [e.g., *Ramanathan et al.*, 1995 for the tropics; *Walsh and Chapman*, 1998 for the Arctic]. Using satellite data, cloud radiative forcing can be inferred at the top of the atmosphere [*Ramanathan et al.,* 1989] and at the surface [e.g. *Zhang et al.*, 1995]. For surface cloud forcing (SCF), surface-based methods are more direct and accurate but provide limited sampling. During SHEBA, surface-based measurements provide precisely the mean radiation fluxes to determine CRF over a complete annual cycle for the SHEBA ice floe.

Surface cloud radiative forcing estimates modeled by *Curry and Ebert* [1992], using climatological cloud properties, showed that the average effect of polar clouds, in comparison to clear skies, is to warm the surface over the annual cycle for all months except July. This warming is primarily due to the absence of incoming solar radiation from late fall to early spring and the high surface albedos associated with ice and snow. The SCF becomes negative for only two weeks in midsummer when the clouds act to cool the surface by reflecting a greater portion of insolation than the underlying surface would under clear skies. Similar results were determined by *Zhang et al.* [1996], using a 1-D radiative transfer model concluding that clouds warm the lower atmosphere and surface causing an earlier onset and faster rate of snowmelt. Satellite estimates of cloud radiative forcing for the Arctic surface have also been reported and similarly show positive cloud forcing (warming) values for most of the year with negative values occurring only during June and July [*Schweiger and Key*, 1994].

In this paper, we examine the impact of Arctic clouds on the surface energy balance of sea ice using data obtained from SHEBA. We extend the concept of "cloud forcing" to include surface turbulent as well as, radiative fluxes. We begin with definitions of cloud forcing and a description of our analysis methods (section 2). In section 3 we describe the instruments and the measurements used in the study. In section 4 we present results of the annual cycle of cloud forcing for radiative and turbulent fluxes. These results are compared with the comprehensive review by *Walsh and Chapman* [1998], who used data obtained from two decades of Russian North Pole stations, satellite-derived results from *Key et al.* [1999], and a regional model from *Curry and Ebert* [1992]. Conclusions are given in section 5.

2. Analysis Methods

Cloud Forcing Definitions

The surface energy balance at the snow/ice-air interface can be written as

$$-C_\delta + R_{sn\_\delta} = R_{sd} - R_{su} + R_{ld} - R_{lu} - H_s - H_l - B \quad (1)$$

where R are radiative fluxes with the subscripts s and l denoting solar and longwave, and d and u denoting downward and upward components. H_s is the sensible heat flux and H_l the latent heat flux for evaporation or sublimation (we use the meteorological convention where these fluxes are positive when cooling the interface). These terms can be measured directly in the atmosphere using micrometeorological methods (see section 3). The conductive flux (positive upward), C_δ, and net solar radiative flux, R_{sn_δ}, are realized at some small depth, δ, just below the interface, and we have assumed that the longwave flux does not penetrate significantly below the surface. The balance term, B, accounts for ice-water phase changes (positive for melting) at the interface. The net radiative flux is defined as the difference between the downwelling and the upwelling radiative fluxes.

Downward and upward solar fluxes are related through the albedo, α,

$$R_{su} = \alpha R_{sd} \quad (2)$$

downward and upward longwave fluxes are related through the surface (interface) temperature, T_s, and the emissivity, ϵ,

$$R_{lu} = \varepsilon\sigma T_s^4 + (1-\varepsilon) R_{ld} \quad (3)$$

To assess the impact of clouds on the surface energy balance, we adopted a cloud forcing metric that is analogous to the cloud radiative forcing parameter first introduced by *Ramanathan et al.* [1989]. Cloud forcing as deduced here gives an indication of the effect clouds have on the surface energy balance in comparison to clear skies. For example, if more radiation reaches the surface when clouds are overhead than when skies are clear, the clouds act to warm the surface (i.e. the thermal effect) and the forcing value is positive. If less radiation reaches the surface when clouds are present versus under clear skies, then clouds act to cool the surface (negative forcing); this is, in essence, the albedo effect. The same formalism can be used to assess the impact of clouds on surface turbulent fluxes.

Cloud forcing provides a simplistic means for characterizing the bulk effect of clouds on the Earth's system. Cloud forcing is defined here (following *Ramanathan et al.* [1989]) as

$$CF = < F > - < F_{clear} > \quad (4)$$

where the brackets denote an average, F is the flux of interest (radiative or turbulent), and F_{clear} is the expected flux if clouds are removed from the column.

Alternatively, cloud forcing can be defined in terms of the difference between the flux when skies are overcast, F_1 (cloud fraction, f=1.0) and when they are clear F_0 (cloud fraction, f=0.0). This approach is the conditional cloud forcing (i.e., the amount the flux changes when a cloud is present) and was used to calculate the forcing from turbulent fluxes. We will follow *Walsh and Chapman* [1998] and refer to this as the maximum cloud forcing, *MCF*,

$$MCF = < F_1 > - < F_0 > \quad (5)$$

If we consider a simple bimodal cloud distribution (i.e., either overcast or clear), then cloud fraction can be considered the fraction of time the sky is overcast. In that case, it is simple to show that

$$CF \approx f * MCF \quad (6)$$

The cloud forcing results presented were calculated using direct measurements of the upward and downward longwave (LW) and shortwave (SW) fluxes and the sensible and latent heat fluxes near the surface as well as, an annual cycle of cloud occurrence measurements from a depolarization lidar and a ceilometer. A radiation model was run to calculate the annual cycle of radiative fluxes under clear skies, as described below.

Clear Sky Radiation Model

Clear sky conditions were infrequent at SHEBA especially during the summer [*Intrieri et al.*, 2001; this issue], thus it was necessary to model the clear sky surface radiation fluxes needed for estimating the cloud

radiative forcing. We initially attempted to use the direct flux observations in cloud-free conditions but this created large statistical sampling errors, particularly for the summer shortwave flux.

The clear sky LW and SW, upwelling and downwelling radiative fluxes were calculated using the Santa Barbara Discrete Ordinate Radiative Transfer (DISORT) Atmospheric Radiative Transfer (SBDART) computer code [*Ricchiazzi et al.*, 1998]. The equations of the plane-parallel radiative transfer equation are solved with the DISORT method [*Stamnes et al.*, 1988]. Both thermally emitted and scattered radiation intensities were computed hourly using 42 atmospheric layers. The SW flux calculations were run from 0.28 to 4.0 micrometers and the LW fluxes from 4.0 to 100.0 micrometers. Inputs for this model included hourly values of latitude and longitude from SHEBA Geophysical Positioning System (GPS) data, interpolated profiles of temperature and relative humidity from atmospheric soundings, and surface albedo measurements from radiometers in addition to a 200 m albedo line. Boundary layer and stratospheric aerosol and all radiatively active molecular species, including ozone, were accounted for using standard profiles internally specified within the model.

A comparison of the clear sky modeled (diamonds) and measured (solid line) downwelling SW and LW fluxes (Wm^{-2}) for a 3 day period in late April 1998 are shown in Figures 1a and b, respectively, illustrating several key points.

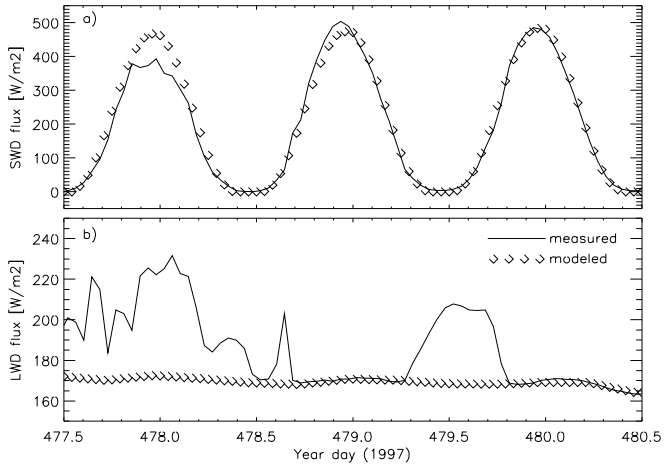

Figure 1. Time series of measured (solid line) and modeled (diamonds) a) downwelling solar flux and b) downwelling LW flux for a three day period in late April, 1998. All in (Wm^{-2}).

On day 478 a cloud was detected by the lidar overhead causing an increase in the downwelling surface LW flux and an associated reduction in the downwelling SW flux. The following day (479) was clear and shows exact correspondence between the modeled clear sky and measured LW flux. Note however, that the measured peak SW downwelling flux is greater than the clear sky modeled values on this day. This is an example of what can happen when frost forms on the PSP dome as was noted in the instrument log for that day. The dome was cleaned shortly before solar noon after which the model and measurements are again in excellent agreement. A cirrus cloud was detected overhead during that evening (479.5), and registers in the downwelling LW trace, but by the next day skies were clear again and both the LW and SW downwelling modeled and measured fluxes correspond. After comparing the downwelling SW modeled and measured peak values for virtually all of the clear sky periods in spring and summer, we determined that it was unnecessary to tune the model results to the observations.

A scatter plot of modeled versus measured downwelling LW fluxes (when cloud fraction = 0) is shown in Figure 2. There is good general 1-1 agreement; however, outliers exist and are attributed to the presence of clouds that were not detected by the vertically pointing sensors or possibly to periods when rime ice formed on the radiometer dome. We contend that the clear sky model under clear sky conditions gives the best estimate of R_{ld_clr}.

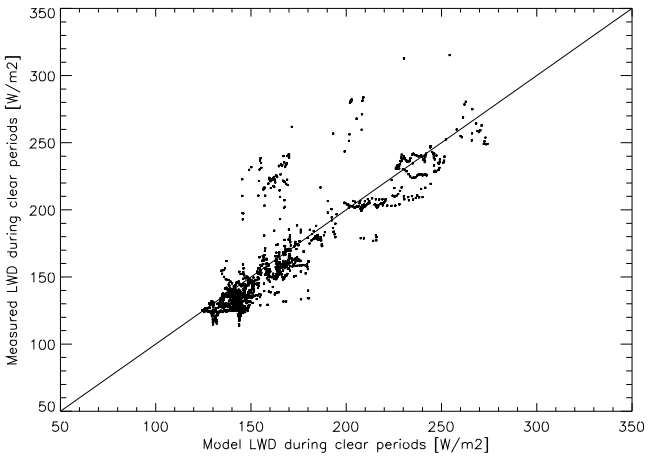

Figure 2. Scatter plot of measured versus modeled downward LW flux (Wm^{-2}) for clear sky periods (cloud fraction = 0.0).

Cloud Fraction, Time Averaging and Albedo Considerations

Determining cloud fraction values, although conceptually simple, is non-trivial and often has several definitions associated with it. True cloud fraction is the instantaneous fraction of the sky covered by clouds and is usually determined by observers or whole sky imaging devices. This definition is distinct from vertical cloud fraction, f, which is usually determined from time or space averages of vertically-oriented, narrow field-of-view cloud sensors (lidar or ceilometer in the case of our analyses). We have chosen the latter approach because observers are subjective and prone to errors in dark conditions and current whole sky imaging technology does not provide information on cloud properties. Here, we averaged six 10-min averages of lidar cloud occurrence data to obtain a 1 hour vertical cloud fraction value. For those time periods when the lidar was inoperable (mid-August through October 1998), the ceilometer was used to determine cloud presence. We concede that our approach is imperfect, mainly because clouds can influence the surface radiation without passing directly in the field of view of the remote sensors. However, Arctic clouds have been shown to have a highly bimodal distribution [*Walsh and Chapman*, 1998; *Makshtas et al.*, 1999], which is most favorable for our simplified approach. The annual cycle of cloud occurrence during SHEBA, averaged over 20 days, is shown in Figure 3.

We illustrate the efficacy of the vertical cloud fraction in Figure 4 where clear periods (0% values, lower panel) are shown to be highly correlated with minima in the downward LW flux (diamonds, upper panel) and overcast periods (100%, lower panel) are associated with maxima (asterisks, upper panel). Partial cloud fractions are indicated with a plus. Intermediate values of the flux are associated with both partial cloud fraction and overcast periods suggesting that cloud microphysics are influencing the observed downward LW flux. Note that SCF does not rely on determining clear or overcast conditions but relies on the accurate specification of the clear sky flux.

Daily values of the flux measurements, clear sky model results and cloud forcing calculations were averaged over the annual cycle in 20-day

blocks. We chose this time interval because it maintains all the annual cycle features while smoothing over any synoptic weather events, extended clear sky periods, and/or periodic instrument inconsistencies. Shorter time intervals were tested (e.g., 5, 10, and 15 days) but rejected due to the reasons cited above.

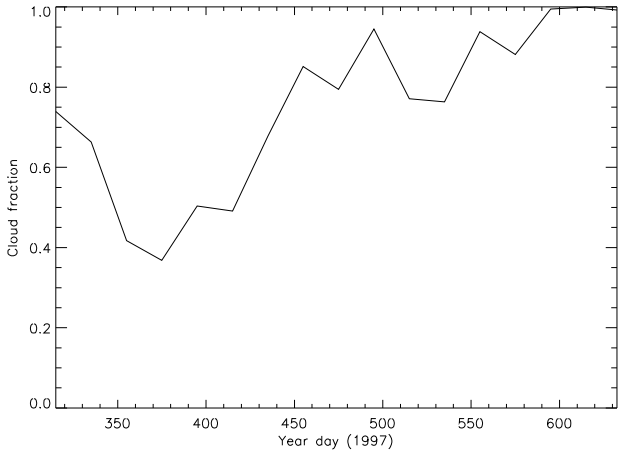

Figure 3. Annual cycle of cloud fraction averaged over 20 day blocks.

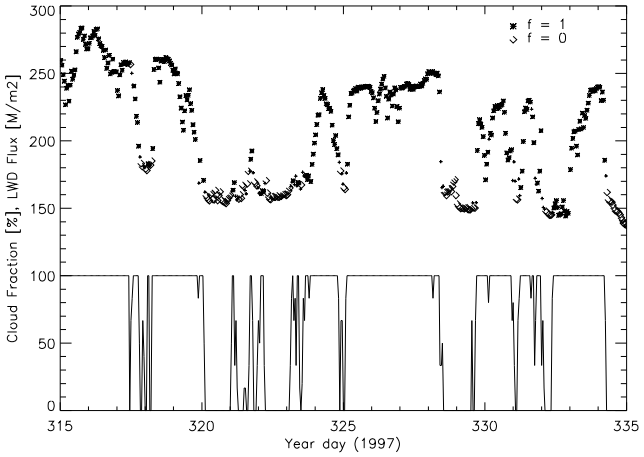

Figure 4. Time series of hourly-averaged downward LW flux in Wm^{-2} (upper panel) where asterisks correspond to overcast skies (cloud fraction =1.0), diamonds to clear skies (cloud fraction = 0.0) and crosses otherwise. Corresponding time series of hourly-averaged cloud fraction (lower panel).

Two different types of albedo measurements were used for running the clear sky model calculations; single site albedos and line-averaged albedos. The former albedo values were computed for each hour over the full annual cycle by the Atmospheric Surface Flux Group (ASFG) radiometers. The radiometers were located at the base of the 20 m tower and were also used for the surface flux measurements. The tower was purposefully located on a stable piece of multi-year ice so that it would not need to be relocated during the melt season. The second set of albedos we used were obtained by the Cold Regions Research and Engineering Laboratory (CRREL) group from May to September, once daily around solar noon, from a 200 m line that incorporated many different ice types including melt ponds and open water [*Perovich et al.*, 2001; this issue]. Figure 5 shows the comparison of the two albedo data sets illustrating the generally lower CRREL values. Note that in early July however (~day 550) , the values converged due to a melt pond which formed within the field of view of the ASFG radiometer. Shortly thereafter, the melt pond refroze and consequently became covered with snow again in late August. For more detail on both albedo data sets refer to *Persson et al.*, [2001a this issue]. The ASFG radiometer albedos are directly related to the observed fluxes, and are temporally more representative, while the CRREL albedos are more spatially representative of the SHEBA ice camp area. In our analysis and discussion presented in section 4, the year long data set of ASFG albedos were used for consistency. The CRREL albedos were used only in a comparison model run to illustrate the sensitivity of SCF to albedo.

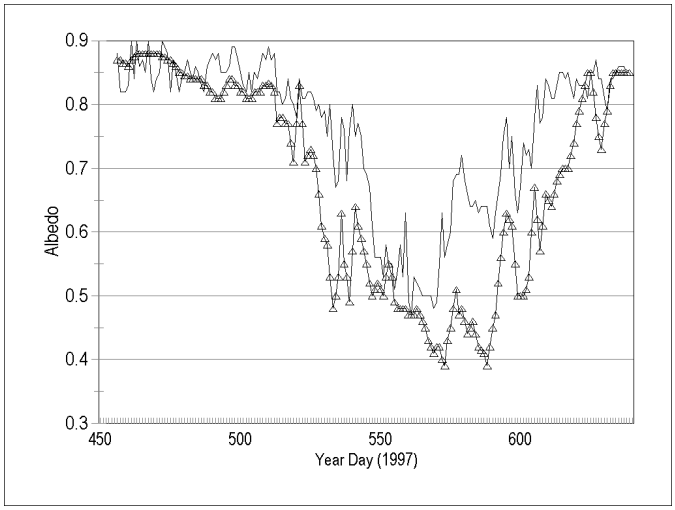

Figure 5. Annual cycle of ASFG albedos (line) and CRREL albedos (asterisks).

3. Measurements and Instruments

Descriptions of the SHEBA experiment, the depolarization lidar [*Alvarez et al.*, 1998], and details regarding the determination of cloud occurrence are described in a companion paper [*Intrieri et al.,* 2001; this issue], which also presents statistics of the annual cycle of cloud geometry and phase. Additional detail discussing surface fluxes can be found in a companion paper by *Persson et al.*, [2001a; this issue]. In this section, we summarize the radiative and turbulent flux measurements and their implications for determining surface cloud forcing.

Infrared and Solar Radiative Flux Measurements

In this study, Eppley Precision Infrared Radiometer (PIR) hemispheric flux pyrgeometers were used to measure the broad band (dome bandpass in the 4.0 - 50.0 μm wavelength range) long wave component, and Eppley Precision Solar Pryanometer (PSP) broadband radiometers were used to obtain the short wave radiative fluxes (dome bandpass in the 0.29 - 2.80 μm wavelength range). While these instruments detect radiation within the stated bandpass, their calibration coefficients are set to return the entire SW or LW component. The radiometers used in this study were deployed and operated by the SHEBA ASFG [*Persson et al.*, 2001b; this issue]. To measure the four radiative components, one PSP and one PIR were mounted to look upward and another radiometer pair to look downward at undisturbed snow. The PIR and PSP measurements from the ASFG were selected from the various radiation flux measurements

because they were determined to have been the most reliable of the conventional radiative flux instruments [*Russell et al*., 1999a] at the SHEBA ice camp. This was, in part, due to the fact that the ASFG radiometer domes were maintained relatively ice-free over the course of the year due to personal attention, proximity to the ship, and the installation of fans at the initial deployment.

The ASFG radiometers were located nominally 2 m above the snow surface, near the base of the 20 m meteorological tower originally set approximately 200 m from the ship. Over the course of the year the ice shifted; by summertime the tower had changed its bearing relative to the ship by ~ 90° and was also displaced by about 300 m. The radiometers were sited in an area that had fairly deep snow by the spring.

The radiometer thermopile outputs and, in the case of PIRs, dome and case temperatures were sampled every 10 s; means and standard deviations were stored at 1 min intervals. These data were averaged to 1 hour intervals to produce time series of upward and downward radiance in Wm^{-2}. The LW flux was computed from the PIR using the methods of *Fairall et al.* [1998]; the SW flux was calculated directly from the PSP thermopile values.

All instruments were calibrated by the NOAA Climate Monitoring and Diagnostics Laboratory prior to and after SHEBA; the calibration coefficients were linearly interpolated in time over the experiment. The PIRs were calibrated in a temperature-controlled blackbody chamber [e.g., *Philipona et al.*, 1995 and 1998], and the PSPs on the roof of the NOAA building in Boulder, CO [*Michalsky et al*., 1997]. *Fairall et al.* [1998] characterize the PIR accuracy as follows: when using laboratory calibrations, a typical unit will have mean bias of about 5 Wm^{-2} with an additional random scatter of 5 Wm^{-2} for 1 hour average values. The mean bias can be reduced by comparing against an absolute standard in the field or an ensemble of PIRs. When compared against edited data from an ensemble of values from five SHEBA ice camp upward facing PIRs, the ASFG unit had a bias of 0.2 Wm^{-2} [*Russell et al.,* 1999b]. The downward facing PIRs cannot be compared because they looked at different surfaces. Thus, we estimate that the mean values produced from the ASFG PIRs have absolute bias accuracies of about ±2.5 Wm^{-2} for both the incoming and outgoing LW components, R_{ld} and R_{lu}, and ±4 Wm^{-2} for R_{lnet}.

Recently, *Bush et al.* [2000] showed that the Eppley PSPs are subject to a negative bias associated with slight transparency of the domes to LW radiation and direct LW coupling of the dome and thermopile (which may not be at the same temperature). Although the ASFG PSPs had a standard radiation shield and the domes were strongly ventilated, both upward and downward flux sensors showed a nighttime bias of -3±2 Wm^{-2}. Negative SW values were set to 0 in post-processing. We estimate our uncertainty in mean downward SW to be ±3% with a bias from -3 to -10 Wm^{-2} and in mean upward SW to be ±3% with a bias of -2 to -5 Wm^{-2}. Mean net SW is uncertain by ±4.5% with a bias of -1 to -7 Wm^{-2} .

Because cloud forcing is essentially the difference in net radiative fluxes, the biases will tend to cancel, unless they are different in clear and cloudy conditions. For LW flux we expect good bias cancellation and estimate the sensor-based uncertainty in mean SCF(LW) to be about 3 Wm^{-2}. Cosine response errors contribute negligibly to our estimates of SCF(SW) because the summer is predominantly cloudy (i.e., the solar radiation is diffuse). We estimate our sensor-based uncertainty in SCF(SW) to be about ±4.5% with a bias of 4 Wm^{-2}.

Turbulent Flux Measurements

Five levels (2 to 18 m nominal height above the surface) of sonic anemometer-thermometers, mounted on the ASFG 20 m tower, were used to compute the turbulent fluxes. The data used include direct turbulent fluxes measured by eddy correlation and estimates of the fluxes based on a bulk transfer algorithm. The data were sampled at 10 Hz and linearly de-trended each hour. The quality of each sonic anemometer 1 hour time series was evaluated on the basis of the streamwise and vertical velocity variances.

Bulk fluxes were computed from measurements of 1 hour mean surface temperature, air temperature, humidity, and wind speed using a modified form of the Coupled Ocean Atmosphere Response Experiment (COARE) sea-air flux algorithm [*Fairall et al*., 1996]. A velocity roughness length of 4.5×10^{-4} m was specified; this gave the best fit to the covariance stress measurements over the annual cycle. Temperature and moisture roughnesses were taken from the snow-ice parameterization of *Andreas* [1987]. Bulk and covariance values agree well, on average, for sensible heat flux; but the bulk values are about twice the covariance values for the latent heat flux. Because the fast hygrometer had not been calibrated for Arctic conditions, we decided to discount the covariance values and use bulk values for the latent heat flux. For sensible heat flux we used the median of the five quality-controlled eddy correlation values. If no valid eddy correlation values were available, we used the bulk value. *Ruffieux et al.* [1995] determined that sensible heat fluxes measured with sonic anemometers were accurate to about ±2 Wm^{-2} for conditions similar to SHEBA. Mean latent heat fluxes were very small (maximum value of 5 Wm^{-2} in June) throughout SHEBA; their uncertainty is less than ±1 Wm^{-2}.

Atmospheric Sounding Measurements

Standard atmospheric profiles of temperature, relative humidity, pressure, wind direction, wind speed, etc. were obtained from the GPS/LORAN Atmospheric Sounding radiosonde system. Sondes were launched at the ice camp during the entire SHEBA experiment at least twice daily (1115 and 2315 UTC), with four daily soundings (0515, 1115, 1715, and 2315 UTC) during the research aircraft overflights conducted from April through July 1998. The system was developed by the National Center for Atmospheric Research and is based on a Vaisala sonde that has a 1 second sampling rate and a reported accuracy of ±0.2 °C for temperature and 2 - 4% for relative humidity (although at the very low temperatures experienced during the SHEBA winter the uncertainty is most likely larger). The atmospheric temperature and humidity profiles were linearly interpolated to an hourly grid for the entire year and used as input for the clear sky model.

4. Annual Cycle of Cloud Forcing

Radiative Fluxes

The annual cycle of downward, upward and net surface SW fluxes are shown in Figures 6a, 6b, and 6c, respectively, where the dashed lines represent clear sky modeled fluxes and the solid lines are the measured fluxes under all conditions. The downwelling shortwave radiation displays the familiar strong seasonal trend with maximum measured surface insolation reaching 300 Wm^{-2} in mid-June (Figure 6a). The decrease in the reflected or upwelling SW flux (Figure 6b), beginning in late June and persisting until late August, is due to the summertime decrease in surface albedo. Net flux values (downwelling minus upwelling) follow accordingly, with the peaks corresponding to time of year with minimum summer albedo values.

Because the Arctic has little or no solar radiation for over half the year, LW radiation plays an important role in the surface energy balance. With atmospheric conditions typically dry, and thus less opaque to LW radiation, the occurrence of clouds significantly increases the LW emission by the atmosphere. The annual cycle of downward, upward and net surface LW fluxes are shown in Figures 7a, 7b, and 7c, respectively, with the same conventions as the SW plots discussed above. The downwelling LW flux is greater when clouds are present in the column over the course of the entire annual cycle (Figure 7a). This is partly due to the fact that low clouds are often warmer than the surface because of strong Arctic temperature inversions. Note the minimum downwelling

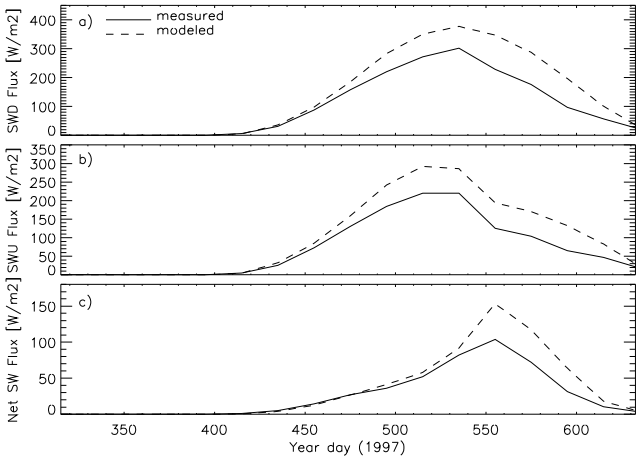

Figure 6. Annual cycle of measured (solid line) and clear sky modeled (dashed line) (a) downwelling solar flux; (b) upwelling solar flux; and (c) the net solar flux. All in Wm^{-2}.

LW values in winter which correspond to the lower observed cloud fractions in addition to very low atmospheric temperatures. The flux differences are essentially zero between clear and cloudy skies in the upwelling LW fluxes (Figure 7b) since the surface temperatures are similarly specified between the model and measurements. (Note: We have already shown that clouds affect surface temperatures in winter. By using observed surface temperatures in our clear sky model calculations, versus only temperature observations during clear periods, our resulting LW cloud forcing may be slightly stronger since our clear sky surface temperatures aren't as cool. This not a consideration in summer and we estimate that it only has a maximum effect in January of 6 Wm^{-2}.) The LW net doesn't change substantially over the annual cycle (Figure 7c) or display a marked seasonal variation like the net SW flux. This is due to the relatively larger difference between the measured downwelling and upwelling LW in winter from strong inversions, and higher cloud fractions in summer. The measured net LW annual cycle only varies over 30 Wm^{-2} with an annual mean of approximately -22 Wm^{-2}.

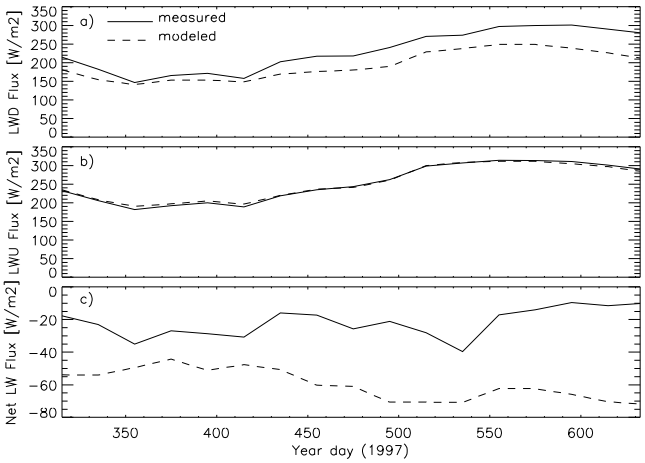

Figure 7. Annual cycle of measured (solid line) and clear sky modeled (dashed line) (a) downwelling LW flux; (b) upwelling LW flux; and (c) the net LW flux. All in Wm^{-2}.

The annual cycle of SW and LW surface cloud forcing for the upwelling (dashed line), downwelling (solid line) and total (the difference of downwelling and upwelling; dash-dot) components are shown in Figures 8a and 8b, respectively. Obviously, when there is no solar contribution during winter the effect of clouds on SCF(SW) is zero (Figure 8a). Progressing toward summer however, albedos steadily decrease and the increasing cloud amount limits the insolation from reaching the surface (cooling effect). The greatest amount of negative SW cloud forcing occurs in late June through early July when the upwelling solar radiation is significantly reduced due to the increase in melt pond fraction and open ocean areas (i.e. decrease in albedo). The SCF(LW) (Figure 8b) is dominated by the downwelling component especially in comparison to the upwelling contribution which is small. Generally clouds warmed the surface relative to clear skies throughout the year but greatest in the late summer and early fall. The annual mean for SCF(SW) is -9 Wm^{-2} and for SCF(LW) is 38 Wm^{-2}. Taking into account the radiometer instrument errors as reported in section 3, the annual means become -9 +/- .5 Wm^{-2} (with a 4 Wm^{-2} bias) for the SCF(SW) and 38 +/- 3 Wm^{-2} for SCF(LW).

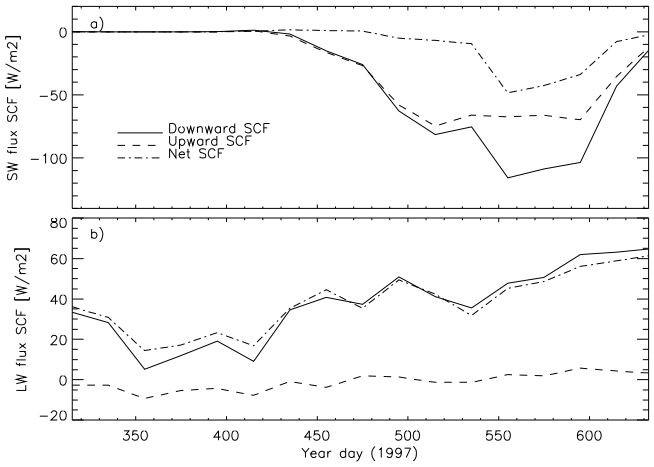

Figure 8. Annual cycle of (a) solar surface cloud forcing; solar downwelling (solid line), solar upwelling (dashed) and the solar net forcing (dash-dot). Annual cycle of (b) LW surface cloud forcing; LW downwelling (solid line), LW upwelling (dashed) and the LW net forcing (dash-dot). All in Wm^{-2}.

Turbulent Fluxes

We sampled the turbulent fluxes over the SHEBA annual cycle for overcast, clear, and mean conditions. Note that no clear sky model exists for near-surface turbulent fluxes. Therefore, the sensible and latent heat fluxes (Figures 9a and 9b) were partitioned and computed for cloud fraction = 1 (solid line) and cloud fraction = 0 (dashed line), in order to determine the MCF (dash-dot) using Equation (5). Unlike the radiative fluxes, turbulent fluxes are primarily determined by the surface-air temperature differences and near-surface wind speed rather than an integral over the entire atmospheric column. Because of the small sample sizes of totally clear or totally cloudy skies in some 20 day periods, large temporal variations in the fluxes occur. Nevertheless, it is obvious that turbulent fluxes warm the surface during clear conditions and are small in cloudy conditions during most of the year.

During July (days 547-577), there was little difference in the sensible heat flux between clear and cloudy conditions. In late May and early June (days 500-540), surface warming and relatively dry atmospheric conditions produced peaks in the latent heat flux for both clear and

cloudy conditions. The MCF for the sensible heat flux was about -6 - -10 Wm^{-2} during the winter and -2 - 0 Wm^{-2} during the summer. The smaller absolute values in the summer indicate that the differences between clear and cloudy conditions in the surface-air temperature difference and wind speed are much smaller in the summer than in the winter. The MCF for H_l ranges from -2 - 0 Wm^{-2} during the winter and spring, decreasing slightly to -3.5 - -1 Wm^{-2} during late spring and summer. Note that the sign convention for the MCF is opposite that for H_s and H_l, so the negative MCF values indicate that the MCF of the turbulent heat fluxes produces surface cooling. Hence, they act opposite the longwave radiative fluxes, but are only significant during the winter. The annual average turbulent flux contribution is -6 Wm^{-2}.

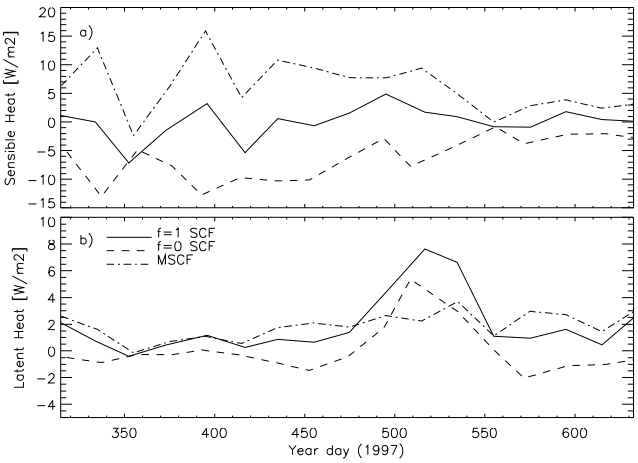

Figure 9. Annual cycle of (a) sensible heat flux and (b) latent heat flux for clear skies (cloud fraction = 0.0, dashed line), overcast skies (cloud fraction =1.0, solid line) and MSCF (cloudy minus clear, dash-dot). All in Wm^{-2}.

Discussion

The annual cycle of cloud forcing for each atmospheric component of the surface energy budget is shown in Figure 10: SW (solid line), LW (dashed line), and the sum of the turbulent fluxes (dash-dot) calculated using Equation (6). This illustrates the relative contributions from each throughout the course of the year. The sum of all the components is shown in Figure 11 (solid line) which represents the annual cycle of *total* Arctic cloud forcing. The dashed line in Figure 11 is the total SCF if the CRREL albedo is used as input for the clear sky model. Both sets of calculations exhibit the same annual cycle trend in cloud forcing; a warming effect in winter, spring and fall and a cooling effect in summer. The SHEBA/ASFG results displayed a minimum forcing value of around -4 Wm^{-2} occurring in early July. Using the lower CRREL albedo measurements in the clear sky model resulted in a much deeper summer cloud forcing lasting from 2 June through August 22. This is due to the fact that, in summer, the relatively higher albedo clouds reflect more SW radiation than the lower albedo surface would under clear skies.

It is important to note that SCF cannot be properly calculated from the CRREL albedo data. The ASFG measurements and subsequent SCF describe the influence of clouds on thick, multi-year ice. The CRREL albedo line, however, covered many ice conditions that varied widely from multi-year ice, and presumably, the upward surface radiation varied across this line as well. In order to accurately calculate SCF for the CRREL albedo line, corresponding flux measurements would be necessary. The inclusion of the CRREL albedos in this study should be viewed in a qualitative sense to demonstrate the influence of lower surface albedos on SCF.

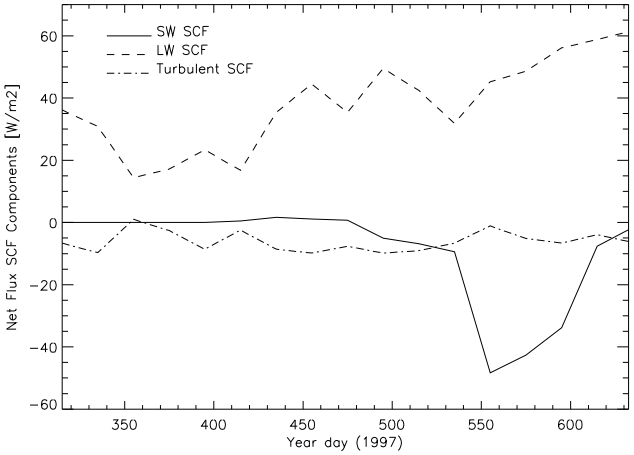

Figure 10. Annual cycle of the net cloud forcing components for solar (solid line), LW (dashed line) and turbulent (sum of latent and sensible fluxes; dash-dot). All in Wm^{-2}.

The increase in the mid-summer CRREL SCF results illustrates an interesting point about the sensitivity of using mismatched albedos and fluxes. In essence, the CRREL albedos, representing the SHEBA area, began to decrease before the observed upwelling SW fluxes at the tower did. This created a falsely larger difference in the SW net fluxes, which caused a substantially sharper negative cloud forcing. When the CRREL and ASFG albedos were similar around day 550 (because a melt pond formed within view of the tower radiometers) the curves become closer. Afterwards, however, the CRREL albedo values became lower once again than the flux measurements would support. This is essentially the case until early September when snow begins to fall in the SHEBA region increasing albedos uniformly across the area.

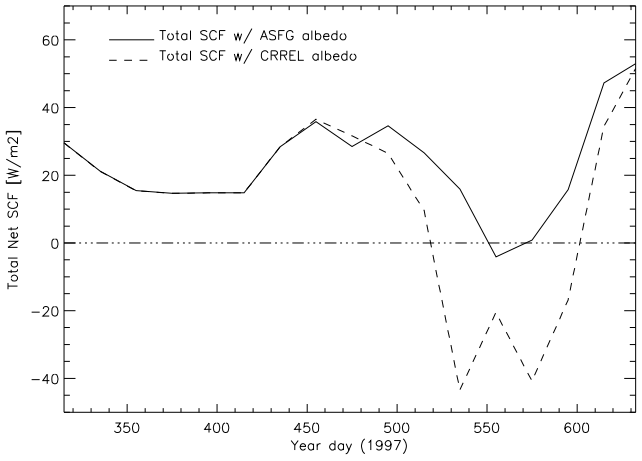

Figure 11. Annual cycle of the total cloud forcing (sum of net solar, net LW, and net turbulent cloud forcing) using the ASFG albedos (solid line) and CRREL albedos (dashed line). All in Wm^{-2}.

In summary, we observed that the atmosphere over SHEBA was predominantly cloudy and that the clouds had a net warming effect on the sea ice surface throughout the entire year except for a short period during summer. In winter and spring, the net cloud forcing is dominated by LW effects due to the absence of SW radiation. In summer however, the SW reflective properties of clouds, combined with the decrease surface albedo, become dominant. This overall cloud induced warming is in contrast to the year round cooling that has been observed to occur at lower latitudes [*Harrison et al.*, 1990] and is a consequence of the absence of solar radiation for a large portion of the year, low humidity in the polar atmosphere, strong and persistent temperature inversions, very low surface temperatures and the highly heterogenous sea ice surface. The annual average of the total SCF is 19 Wm^{-2} (+/- 3 Wm^{-2}; incorporating the SCF(LW), SCF(SW), and turbulent flux accumulated instrument error and bias) using the ASFG albedos and 12 Wm^{-2} using the CRREL albedos.

In Figure 12 we compare our SHEBA cloud forcing results using the ASFG albedos (solid line) and the CRREL albedos (dash-dot line) with model results from *Curry and Ebert* [1992, hereafter CE] (diamonds), summary data from *Walsh and Chapman* [1998, hereafter WC] using the Russian North Pole (NP) drifting stations (triangles), and satellite results derived from ISCCP (International Satellite Cloud Climatology Project) "D" cloud data from *Key et al.* [1999, hereafter K] (asterisks). Generally, the annual trend of winter warming and summer cooling is observed in each of these datasets. There are differences in the depth of the summer SCF's which can in part be attributed to differences in albedo and solar zenith angles. Even a small difference in solar zenith angle at high latitudes can contribute to large discrepancies. Wintertime values, without influence from these solar considerations, compare well between the SHEBA and WC results. The CE model and the K satellite results are larger during winter by a factor of approximately two. All results show a rather abrupt summer-fall transition. The CE model results, however, show a much later transition into the melt season than the observations indicate which is partly due to their later specification of the melt season. The annual average radiative SCF is 23 Wm^{-2} for the SHEBA/ASFG data, 12 Wm^{-2} for the SHEBA/CRREL data, 38 Wm^{-2} for the CE model, 13 Wm^{-2} for the K satellite data and 4.5 Wm^{-2} for the WC Russian drifting stations.

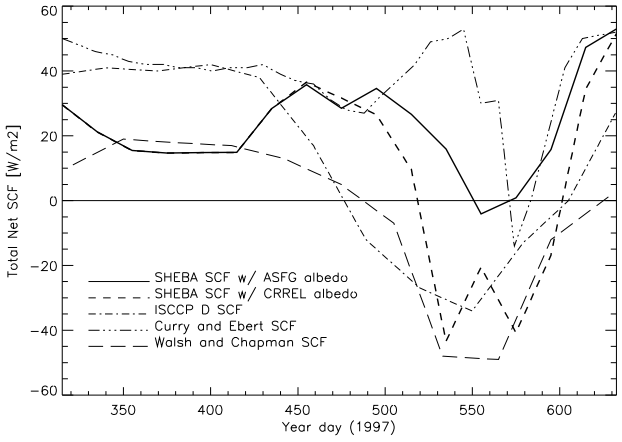

Figure 12. Comparison of SHEBA total cloud forcing data using the ASFG albedos (solid line) and CRREL albedos (dash-dot) with data from Walsh and Chapman [1998] (triangles), model results from Ebert and Curry [1992] (diamonds) and satellite-derived results from Schweiger and Key [1994] (asterisks). All in Wm^{-2}.

5. Summary and Conclusions

Characterizing cloud radiative effects in the Arctic is a critical component for understanding the current polar climate and an important step towards simulating potential climate change in polar regions. Cloud forcing is a simple and effective means of evaluating the impact of clouds on the surface energy balance. In this study, we present the Arctic surface cloud forcing calculated over an annual cycle using measurements from ground-based remote and in situ sensors deployed as part of SHEBA and a radiative transfer model. The measurements incorporated in this study included those from optical radiometers, a depolarization lidar, a ceilometer, and radiosondes.

The results show that, over the course of the year, the net effect of Arctic clouds is to warm the surface with a slight cooling effect present for a short period during summer. This summer cooling results because the surface albedo is low and clouds act to reduce the downwelling solar flux. We presented two determinations of SCF calculated using different albedo datasets; one representing the SHEBA ice camp area with lower values and the other a single point measurement which was typically higher. Our best estimates of the annual average SCF are 38 Wm^{-2} for LW and -6 Wm^{-2} for turbulent fluxes. For the annual average SCF(SW) we obtained -9 Wm^{-2} using the single-site radiometer albedos and -21 Wm^{-2} using the area-averaged albedos.

Comparisons were made with model, satellite, and Russian drifting station data showing generally good agreement in the annual cycle trend but marked differences in magnitude. During summer, this is not surprising given that even small differences in solar parameters, such as zenith angles and albedos can produce large discrepancies. Wintertime values, however, were most similar between the SHEBA and drifting station datasets but were half as much as the satellite and model results.

With the addition of lidar and microwave radiometer measurements we also have concurrent cloud property information such as liquid water content, cloud phase and base height. We are currently combining the cloud forcing data presented here with the cloud property data to better understand how and which clouds contribute most and during what seasons to the surface energy balance. For example, we have determined that winter clouds containing liquid water phase influence surface warming the most. Additional microphysical information, provided by radar and lidar retrievals, for example, could allow us to understand relationships between cloud particle sizes or liquid water contents on surface fluxes and potentially to understand one possible feedback event. Specifying cloud parameters correctly in models will be one critical factor for assessing cloud impact in the Arctic.

With this baseline of measurements, we can begin to extrapolate and experiment with different cloud scenarios, such as increasing or decreasing cloud amount or the percentage of clouds in liquid phase, to understand how evolving cloud conditions may affect sea ice. The complications involved in assessing a comprehensive cloud-radiation feedback effect remain a challenge. Data sets such as these, however, provide a starting point for gauging the performance of models in capturing the correct shape and sign of seasonal trends.

Acknowledgments. This work was supported by NASA FIRE.ACE program under contract # L64205D, the NSF SHEBA program under agreement # OPP-9701730 and the NASA EOS Validation Program under contract # S-97895-F. We would like to thank the program managers Bob Curran, Michael Ledbetter and David O'C Starr respectively. The authors also acknowledge the many people who participated in the incredible task of deploying and maintaining the lidar and radar systems under harsh environmental conditions for an entire year including Jeff Otten, Scott Sandberg, Raul Alvarez, Duane Hazen, Peter Guest, Marty Mulhern, Ann Keane, Dave Costa, and the crew of the C.C.G.C Des Groseilliers. We would also like to thank Keith Koenig, Joanne George, Wendi Madsen, and Kathleen Healy for their programming contributions.

References

Alvarez, R.J., II, W.L. Eberhard, J.M. Intrieri, C.J. Grund, and S.P.Sandberg, A depolarization and backscatter lidar for unattended operation in varied meteorological conditions, *Proc. 10th Symp. on Meteor. Obs. and Instrumentation*, 140-144, 1998.

Andreas, E.L, A theory for the scalar roughness and the scalar transfer coefficients over snow and sea ice, *Bound.-Layer Meteorol.,* 38, 159-184, 1987.

Beesley, John A., Estimating the effect of clouds on the arctic surface energy budget, *J. Geophys. Res.,* 105, 10,103-10,117, 2000.

Bush, B. C., F. P. J. Valero, and A., S. Simpson, Characterization of thermal effects in pyranometers: a data correction algorithm for improved measurement of surface insolation, *J. Atmos. Oceanic Technol.*, accepted, 2000.

Curry, J.A., and E.E. Ebert, Annual cycle of radiative fluxes over the Arctic Ocean: Sensitivity to cloud optical properties, *J. Clim.*, 5, 1267-1280, 1992.

Curry, J.A., J.L. Schramm, and E.E. Ebert, Impact of clouds on the surface radiation balance of the Arctic Ocean, *Meteorol. Atmos. Phys.*, 51, 197-217, 1993.

Curry, J.A., W.B. Rossow, D. Randall, and J.L. Schramm, Overview of Arctic cloud and radiation characteristics, *J. Clim.,* 9, 1731-1764, 1996.

Curry, J.A., et al., FIRE Arctic Clouds Experiment, *Bull. Amer. Meteorol. Soc.*, 81, 5-29, 2000.

Fairall, C. W., E. F. Bradley, D. P. Rogers, J.B. Edson, and G.S. Young, Bulk parameterization of air-sea fluxes for TOGA COARE. *J. Geophys. Res.*, 101, 3747-3767, 1996.

Fairall, C.F., P.O.G. Persson, E.F. Bradley, R.E. Payne, and S.P. Anderson, A new look at calibration and use of Eppley precision infrared radiometers, Part I: Theory and Application, *J. Atmos. Oceanic Technol.,* 15, 1229-1242, 1998.

Harrison, E.F., et al., Seasonal variations of cloud radiative forcing derived from the Earth Radiation Budget Experimnet, *J. Geophys. Res.*, 95, 18,687-18,703, 1990.

Intrieri, J.M., M.D. Shupe, B.J. McCarty, and T. Uttal, Annual cycle of Arctic cloud geometry and phase from radar and lidar at SHEBA, *J. Geophys. Res.*, this issue, 2001.

Key, J., D. Slayback, C. Xu, and A. Schwieger, New climatologies of polar clouds and radiation based on the ISCCP D products, *Proc. 5th Conf. on Polar Meteorology and Oceanography,* 227-232, 1999.

Makshtas, A.P., E.L. Andreas, P.N. Svyashchennikov, V.F. Timachev, Accounting for clouds in sea ice models, *Atmos. Res.,* 52, 77-113, 1999.

Michalsky, J., M. Rubes, T. Stoffel, M. Wesely, M. Splitt, and J. DeLuisi, Optimal measurement of surface shortwave irradiance usng current instrumentation - The ARM experience, Proc. 9th Conf. On Atmospheric Radiation, J5-J9, 1997.

Perovich, D., K., et al., The Surface Heat Budget of the Arctic Ocean, *EOS Newsletter*, 1999.

Perovich, D.K., T.C. Grenfell, B. Light, and P.V. Hobbs, The seasonal evolution of Arctic sea ice albedo, *J. Geophys. Res.*, this issue, 2001.

Persson, P. Ola G., C.W. Fairall, E.L Andreas, P. Guest and D. Perovich, Measurements near the Atmospheric Surface Flux Group tower at SHEBA Part I: Site description, data processing, and accuracy estimates. *J. Geophys. Res.*, this issue, 2001a.

Persson, P. Ola G., C.W. Fairall, E.L Andreas, and P. Guest, Measurements near the Atmospheric Surface Flux Group tower at SHEBA Part II: Near-surface conditions and surface energy budget. *J. Geophys. Res.*, this issue, 2001b.

Philipona, R., C. Frohlich, and C. Betz, Characterization of pyrgeometers and the accuracy of atmospheric long-wave radiation measurements, *Appl. Opt.,* 34, 1598-1605, 1995.

Philipona, R., et al., The Baseline Surface Radiation Network pyrgeometer round-robin calibration experiment, *J. Atmos. Oceanic Technol.*, 15, 687-696 1998.

Ramanathan, V., R.D. Cess, E.F. Harrison, P. Minnis, B.R. Barkstrom, E. Ahmad, D. Hartman, Cloud-radiative forcing and climate: Results for the Earth Radiation Budget Experiment, *Science*, 243, 57-63, 1989.

Ramanathan, V., B. Subasilar, G.J. Zhang, W. Conant, R.D, Cess, J.T. Keihl, H. Grassl, and L. Shi, Warm pool heat budget and shortwave cloud forcing: A missing physics? *Science,* 267, 499-503, 1995.

Randall, D.A., et al., Status of and outlook for large-scale modeling of atmosphere-ice-ocean interactions in the Arctic, *Bull. Amer. Meteorol. Soc.,* 79, 197-219, 1998.

Ricchiazzi, Paul, Shiren Yang, Catherine Gautier, David Sowle, SBDART: A Research and Teaching Software Tool for Plane-Parallel Radiative Transfer in the Earth's Atmosphere. *Bull. Amer. Meteorol. Soc.*, 79, 2101–2114, 1998.

Ruffieux, D., P.O.G. Persson, C.W. Fairall, and D.E. Wolfe, Ice pack and lead surface energy budgets during LEADEX 1992, *J. Geophys. Res.,* 100, 4593-4612, 1995.

Russell, C.A., C.W. Fairall, P.O.G. Persson, E.L. Andreas, P.S. Guest, R. Lindsay, H.A. Eide, and T. Horst, Intercomparison of downward longwave flux measurements during the first two months of SHEBA, *Proc. 5th Conf. on Polar Meteorology and Oceanography*, 314-318, 1999a.

Russell, C.A., C.W. Fairall, P.O.G. Persson, E.L. Andreas, P.S. Guest, R. Lindsay, and T. Delaney, Intercomparison and normalization of five Eppley pyrgeometer downwelling IR fluxes during April-May, 1998 at SHEBA, *Proc. 10th Conf. on Atmospheric Radiation*, 442-446, 1999b.

Schweiger, A.J. and J.R. Key, Arctic Ocean radiative fluxes and cloud forcing estimates from the ISCCP C2 cloud dataset, 1983-1990, *J. Appl. Meteor.*, 33, 948-963, 1994.

Shine, K.P., Parameterization of shortwave flux over high albedo surfaces as a function of cloud thickness and surface albedo, *Quart. J. Roy. Meteor. Soc.,* 110, 747-764, 1984.

Stamnes, K., S. Tsay, W. Wiscombe, and K. Jayaweera, Numerically stable algorithm for discrete-ordinate-method radiative transfer in multiple scattering and emitting layered media, *Appl. Opt.*, 27, 2502-2509, 1988.

Tao, X., J.E. Walsh, and W.L. Chapman, An assessment of global climate models simulation of Arctic air temperatures, *J. Clim.*, 9, 1060-1076, 1996.

Walsh, J.E., and W.L. Chapman, Arctic cloud-radiation-temperature associations in observational data and atmospheric reanalyses, *J. Clim.*, 11, 3030-3044, 1998.

Washington, W.M. and G.A. Meehl, Climate sensitivity due to increased CO_2: Experiments with a coupled atmosphere and ocean general circulation model, *Climate Dyn.,* 4, 1-38, 1989.

Zhang, Y.C., W.B. Rossow, and A.A. Lacis, Calculation of surface and top of atmosphere radiative fluxes from physical quantities based on ISCCP datasets, Part I: Method and sensitivity to input data uncertainties, *J. Geophys. Res.,* 100, 1149-1165, 1995.

Zhang, T., K. Stamnes, and S.A. Bowling, Impact of clouds on surface radiation fluxes and snowmelt in the Arctic and Subarctic, *J. Clim.*, 9, 2110-2123, 1996.